Electrochimica Acta 353 (2020) 136616

Contents lists available at ScienceDirect

Electrochimica Acta

journal homepage: www.elsevier.com/locate/electacta

# Hydrogen oxidation reaction response of noble-metal based bulk metallic glasses

Vahid Hasannaeimi [1], Chun-Yu Lin [1], Zhenhai Xia, Sundeep Mukherjee*

*Department of Materials Science and Engineering, University of North Texas, Denton, TX, 76203, USA*

ARTICLE INFO

*Article history:*
Received 30 April 2020
Received in revised form
2 June 2020
Accepted 9 June 2020
Available online 14 June 2020

*Keywords:*
Metallic glass
Fuel cell
Electrocatalyst
Density functional theory
Scanning electrochemical microscopy

ABSTRACT

Noble-metal based metallic glasses have recently shown excellent performance towards a range of catalytic reactions, which is attributed to their disordered atomic structure and high density of active sites on the surface. An in-depth understanding of the mechanisms that promote the catalytic performance of amorphous alloys would facilitate the design and development of highly efficient catalysts with significantly lower precious metal loading. In the present study, the electro-catalytic behavior of amorphous Pt- and Pd-based metallic glasses was studied towards hydrogen oxidation reaction by cyclic voltammetry and scanning electrochemical microscopy. The electrochemically active surface area for the metallic glasses was found to be several folds higher compared to pure Pt and Pd. Density functional theory calculations showed that hydrogen oxidation on the surface of the amorphous alloys preferentially followed the reverse Heyrovsky-Volmer pathway. The minimum over-potential for the amorphous alloys was calculated to be significantly lower compared to pure Pt and Pd, consistent with the experimental trends. The enhanced catalytic activity for the amorphous alloys was attributed to the reduced chemisorption of hydrogen on the metallic glass surface, particularly for the alloys containing both Pt and Pd.



## 1. Introduction

Increased impact of climate change has resulted in a strong drive towards cleaner and more sustainable energy resources as a replacement for conventional fossil fuels [1]. Hydrogen is believed to be one of the cleanest and the most promising energy sources of the current century [2,3]. Proton-exchange membrane (PEM) fuel cells using hydrogen have multiple attractive attributes that make them the leading candidates for transportation and portable electronic applications [4]. These include low operating temperature, light weight, long stack life, fast start-up, higher energy density compared to batteries, and potential for lower cost and volume. Expedited hydrogen oxidation reaction (HOR) and oxygen reduction reaction (ORR) over the anode and cathode surface of a PEM fuel cell, respectively, is critical in achieving high efficiency and output power. This requires efficient and inexpensive catalyst design and development for achieving high electro-catalytic activity in the aforementioned reactions. Platinum and palladium-based nano-materials have been reported to be the most effective electro-catalysts for hydrogen oxidation reaction (HOR) [4–6]. Although great progress has been made in PEM fuel cell science and technology, widespread commercialization is still hindered by sluggish kinetics of oxidation/reduction reactions and durability and cost of state-of-the-art catalysts. Development of active, durable, and less expensive electro-catalysts for PEM fuel cell reactions remain as key steps in the realization of fuel cell economy [7].

In an effort to enhance the performance and durability of the catalysts while keeping the precious metal content as low as possible, several pathways have been introduced during the last decade including alloyed and impregnated catalysts [8,9], core-shell structures [10,11], atomic layer catalysts [12], nano-structured catalysts [13,14], and more recently metallic glass catalysts [15–17]. Due to the disordered non-equilibrium atomic structure and high density of low-coordination surface sites, the recently developed amorphous Pt/Pd-based catalysts could be promising alternatives for enhanced catalytic reactions. As opposed to conventional crystalline catalysts in which the catalytic reaction is favored along limited crystallographic orientations, amorphous alloys act as atomic catalysts where each surface site is potentially

* Corresponding author.
*E-mail address:* sundeep.mukherjee@unt.edu (S. Mukherjee).
[1] Equally contributing authors.

https://doi.org/10.1016/j.electacta.2020.136616
0013-4686/

active for chemical species oxidation/reduction [16,17]. Metallic glasses may be thermo-plastically processed into hierarchical nano-structures [18] that possess high electrochemically active surface area and better durability compared to state-of-the-art Pt/C [19,20]. So far, metallic glasses have shown excellent performance as catalysts in hydrogen evolution [20], methanol electro-oxidation [15,21], and other heterogeneous catalytic reactions [22].

Design of next generation metallic glass catalysts requires fundamental understanding of the link between the chemistry (or composition) of the alloy and its catalytic activity given they all have similar amorphous structures. Furthermore, there is no clear understanding of the correlation between amorphous chemistry variation, electro-catalytic activity, and adsorption strength of the chemical species involved in the oxidation/reduction reactions. Here, hydrogen oxidation was studied as the primary anodic reaction in PEM fuel cell for several metallic glasses through cyclic voltammetry and in-situ electrochemical methods. These metallic glasses had varying amounts of Pt and Pd and could be cast into fully amorphous form in bulk dimensions demonstrating excellent glass forming ability. A correlation between adsorption energy and electrocatalytic activity was established using density function theory (DFT) calculations at different levels of hydrogen coverage on the catalyst surface. The synergistic effect of Pt and Pd towards HOR was evaluated for the amorphous alloys containing both the noble metals.

## 2. Materials and methods

### 2.1. Materials

Four recently developed fully amorphous bulk metallic glasses (BMGs) based on Pt and Pd were chosen for this study including a Pt-based bulk metallic glass of composition $Pt_{57.5}Cu_{14.7}Ni_{5.3}P_{22.5}$ [23] (referred to as $Pt_{57}Pd_0$), a Pd-based BMG of composition $Pd_{43}Ni_{10}Cu_{27}P_{20}$ [24] (referred to as $Pd_{43}Pt_0$), and two BMGs containing both Pt and Pd, namely $Pd_{27.5}Pt_{20.9}Cu_{22.6}Ni_{8.2}P_{20.9}$ (referred to as $Pd_{28}Pt_{21}$) and $Pd_{36.1}Pt_{9.2}Cu_{25.1}Ni_{9.2}P_{20.3}$ (referred to as $Pd_{36}Pt_9$). Using high purity starting elements, the alloys were made in the form of amorphous rods by induction melting in vacuum-sealed quartz tubes after appropriate $B_2O_3$ fluxing. The quartz tubes containing molten samples were then water quenched to obtain the amorphous alloys. The chemical composition of the alloys was characterized using a FEI Quanta 200 scanning electron microscope (SEM) equipped with energy dispersive X-ray spectroscopy (EDS). The crystallinity of the alloys was evaluated using a high-resolution X-ray diffractometer (Rigaku Ultima III) with Cu-Kα radiation ($\lambda = 1.54056$ nm) at a voltage of 20 kV. Differential scanning calorimetry (DSC-Netzsch) with a heating rate of 20 K/min was used to obtain the glass transition ($T_g$) and crystallization ($T_x$) temperatures.

### 2.2. Electrochemical measurements

Cyclic voltammetry (CV) was used for measuring the electrocatalytic performance of the metallic glasses in a standard three-electrode cell using a potentiostat/galvanostat (Gamry Ref-3000) with Pt wire as counter electrode, Ag/AgCl (3 M) electrode as reference, and each alloy as a working electrode. Pure Pt and Pd were used as reference materials for comparison. All the CVs were conducted in $N_2$-saturated 0.01 M $H_2SO_4$ + 0.1 M $Na_2SO_4$ electrolyte with a scan rate of 20 mV/s at room temperature. Electrochemically active surface area (ECSA) for each metallic glass was determined from the corresponding cyclic voltammogram by the charge associated with hydrogen adsorption normalized by the weight percentage of noble metal. For side by side comparison of the catalytic activity of the alloys in the same experimental setup, high resolution scanning electrochemical microscopy (SECM, VersaSCAN-AMETEK) was used in collection-generation mode. All the alloys were scanned and monitored in a single run to eliminate any variability associated with the electrolyte and other experimental factors. All the samples were mounted in hard resin and polished to a 0.1 μm surface finish using grinding paper followed by Vibromet polishing for 24 h in 0.04 μm colloidal silica suspension to achieve identical surface roughness for all the alloys. A Pt/Ir (80/20) ultra-microelectrode (UME) with a diameter of 10 μm surrounded with a borosilicate glass tube was used for the measurements. The cyclic voltammetry and SECM experiments were done under identical conditions of the electrolyte to allow for direct comparison between the two methods. The acid medium also helped in achieving higher proton concentration and electrolyte conductivity, better contrast of catalytic activity, and higher signal-to-noise ratio for SECM imaging. Initially, a series of CVs were performed with the UME as the working electrode while it was placed far from the sample surface ( $> 1\ mm$) in deaerated $H_2SO_4 + Na_2SO_4$ electrolyte to find the appropriate potential for maximum hydrogen ($H_2$) generation at the tip. The tip current reached steady state at a potential of $-1200\ mV$ (vs. Ag/AgCl) during the cathodic potential sweep and recorded the highest current for hydrogen reduction. To determine the tip to substrate distance, the polarized tip was slowly brought closer to the substrate and the non-conductive neighboring area to measure the approach curves. The normalized tip current was close to zero when the tip approached the non-conductive region and there was no electrocatalytic activity. On the other hand, the normalized current increased significantly as the tip approached the metallic glass surface due to the oxidation of $H_2$ at the tip (positive feedback from the substrate). The response towards HOR varied depending on the tip to substrate separation for each alloy, as shown in the UME tip voltammograms for $Pt_{57}Pd_0$ in Fig. 1a as an example. The normalized tip current with respect to the tip current in the bulk electrolyte ($UME\ tip_{i_{bulk}}$)showed an almost 12-fold increase when the tip to substrate separation was reduced from 50 μm to 5 μm. A fixed tip to sample separation of ~5 μm was chosen in which there was a large difference between the two approach curves. The tip potential and tip to substrate separation were kept fixed at these values during the scan over the different metallic glass surfaces. Several line scans with a step size of 10 μm were recorded using the polarized UME over the metallic glass catalysts to ensure repeatability of the readings. The SECM setup to measure the electro-catalytic activity of the amorphous alloys along with pure Pt and Pd mounted side by side is shown in Fig. 1b.

### 2.3. Computational models

A series of molecular models were developed to simulate hydrogen oxidation reaction on fully amorphous alloys identical to the Pt/Pd-based metallic glasses used in the experiments. In the models, a vacuum spacing of at least 20 Å was set in the z-direction. Density functional theory (DFT) calculations were carried out using soft projector-augmented wave (PAW) pseudopotentials [25,26] and the Perdew-Burke-Ernzenhof (PBE) [26] exchange correlation functional, as implemented in the VASP code [27,28]. The k-point setting of the Brillouin zone was obtained by 5 × 5 × 1 grid generating meshes with their origin at the gamma point. The plane wave kinetic energy had high cut-off energy of 500 eV throughout the computation. Moreover, all the spin-polarized calculations converged to 0.01 eV $Å^{-1}$ for all surfaces and geometries.

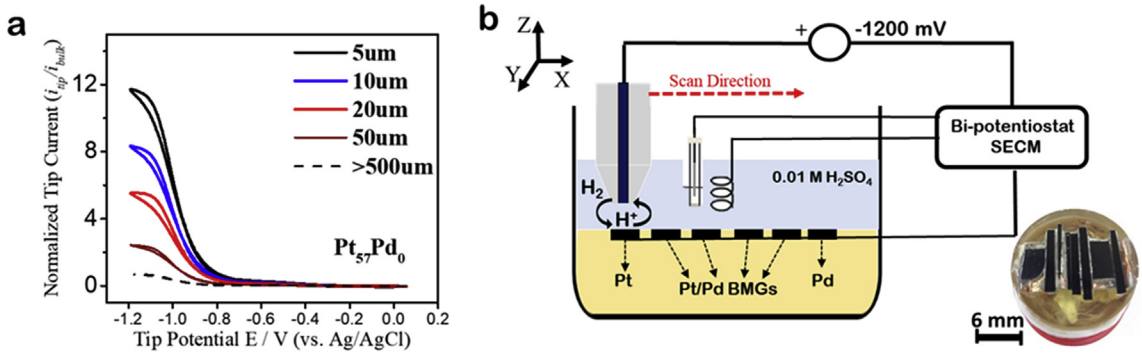


**Fig. 1.** (a) Normalized tip current in the electrolyte at different tip to substrate separation for $Pt_{57}Pd_0$ metallic glass. The tip potential was scanned between −1.2 V and 0.1 V (vs Ag/AgCl) at 20 mV/s, while the substrate was held at OCP; (b) Schematic representation of the scanning electrochemical microscopy (SECM) setup is shown on the left to evaluate the electro-catalytic activity of all the amorphous alloys mounted side by side as shown in the image to the right along with the scale-bar.

## 3. Results and discussion

### 3.1. Structure and thermal stability of the metallic glasses

X-ray diffraction patterns for the as-cast Pt- and Pd-based metallic glass rods are shown in Fig. 2a. Broad diffraction peaks were seen for all the alloys indicating a fully amorphous structure. DSC analysis was performed to determine the thermal stability and crystallization behavior of the glassy alloys in the temperature range of 150 °C–500 °C as shown in Fig. 2b. All the alloys showed a distinct glass transition ($T_g$) followed by super-cooled liquid region and then exothermic reaction corresponding to crystallization ($T_x$). The Pt-based alloy ($Pt_{57}Pd_0$) showed the lowest glass transition temperature followed by $Pd_{28}Pt_{21}$, $Pd_{36}Pt_9$, and then Pd-based BMG ($Pd_{43}Pt_0$). The large difference between crystallization and glass transition temperatures for all the four alloys supports their excellent glass forming ability and thermal stability in the super-cooled liquid region.

### 3.2. Electrochemical characterization

Cyclic voltammetry was employed to investigate the electro-catalytic activity of the metallic glasses toward hydrogen oxidation in 0.01 M $H_2SO_4$. The Pd- and Pt-based metallic glasses showed much higher reactivity compared with elemental pure Pt and Pd (Fig. 3a and b). Pt–H under-potential deposition for pure Pt, $Pt_{57}Pd_0$, and $Pd_{28}Pt_{21}$ was observed in $0.01 < E(V) < 0.2$ (vs Ag/AgCl) and hydrogen adsorption was in the potential range of $E(V) < 0.01\ V$. Potentials higher than 0.5 V were identified as Pt-oxide region. Both $Pt_{57}Pd_0$ and $Pd_{28}Pt_{21}$ showed higher hydrogen oxidation peak currents compared to pure Pt. Furthermore, $Pd_{28}Pt_{21}$ demonstrated a higher oxidation peak than $Pt_{57}Pd_0$ although its' overall noble-metal content was lower. Fig. 3b shows the voltammogram for pure Pd compared to $Pd_{36}Pt_9$ and $Pd_{43}Pt_0$. A similar profile for hydrogen adsorption/desorption has been reported for Pd-based catalysts [29–31]. Hydrogen desorption showed a relatively broad peak for $Pd_{36}Pt_9$ in the positive scan similar to that reported for crystalline catalysts containing Pt and Pd [32]. The metallic glasses containing both Pd and Pt showed very similar behavior towards hydrogen oxidation. High resolution scanning electrochemical microscopy (SECM) [33] was employed to compare the performance of the amorphous catalysts with respect to pure Pd and Pt [34] under identical conditions of electrolyte, pH, temperature, and exposed surface area. The hydrogen oxidation reaction was studied in a deaerated solution containing a high concentration of protons ($H^+$) identical to the electrolyte used for cyclic voltammetry. Higher hydrogen concentration was measured by the UME tip for the more active alloy compositions which resulted in higher recorded tip current. The recorded current at the UME tip was attributed solely to the electrochemical activity of the catalyst since all the alloys were mounted side by side and had a similar surface finish and morphology. A series of line scans were recorded with the fixed parameters and small step size (of 10 μm) and some of the results are plotted in Fig. 3c. The average UME tip

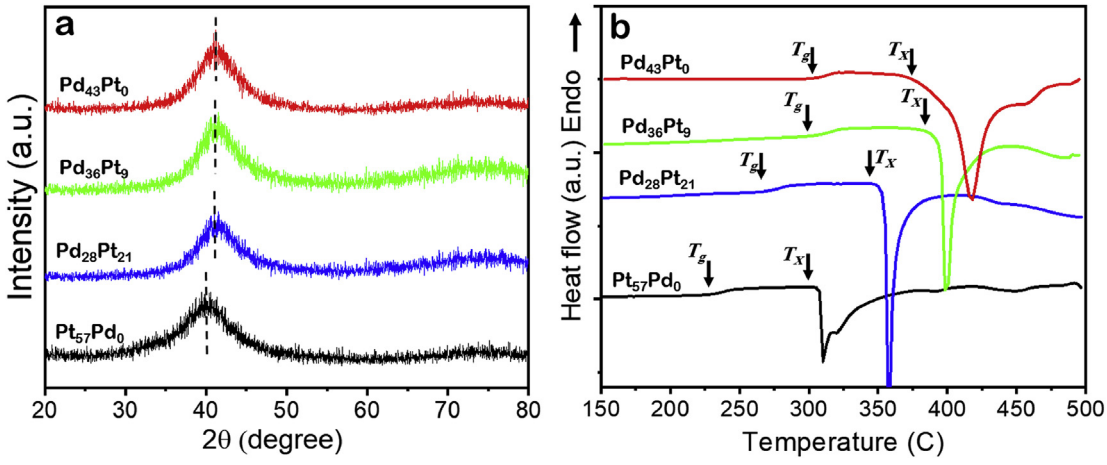


**Fig. 2.** (a) XRD patterns for the Pt- and Pd-based metallic glasses; (b) DSC curves of the metallic glasses at a heating rate of 20 K/min.

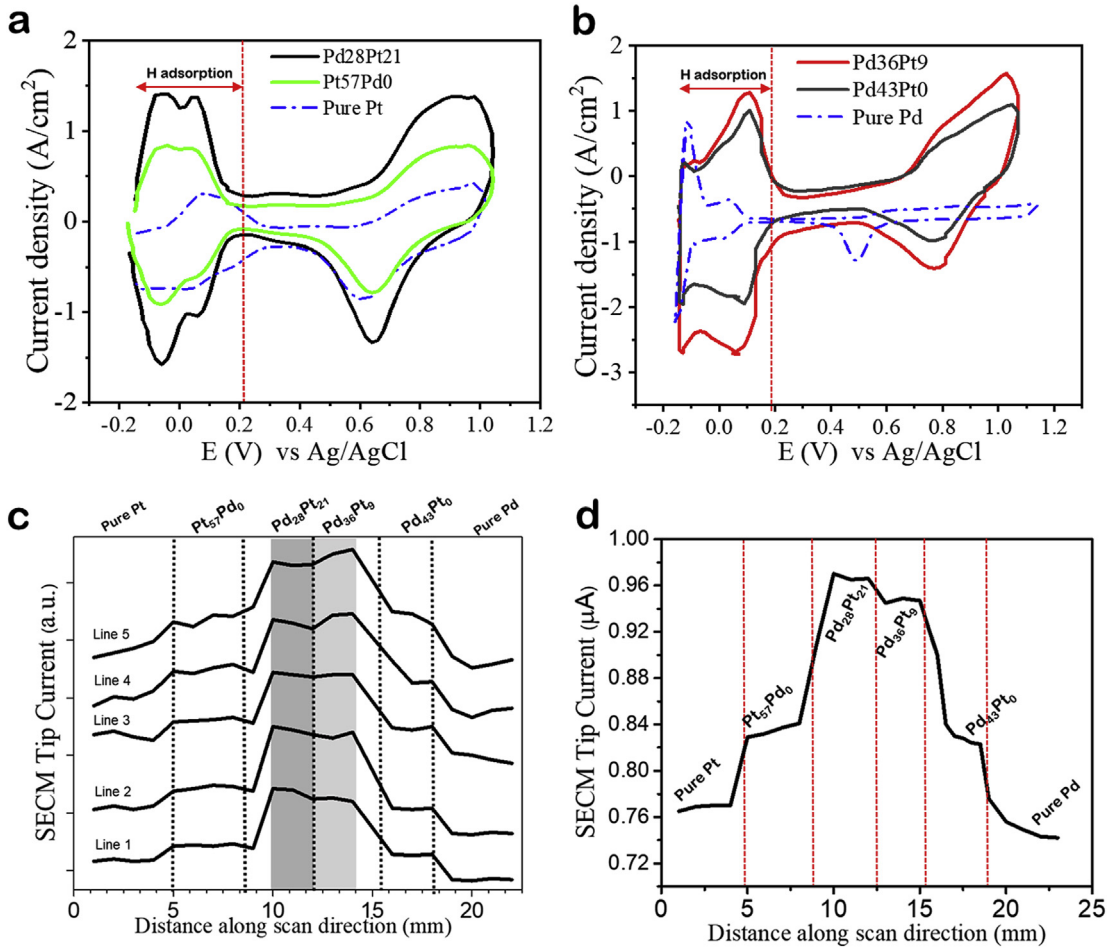


**Fig. 3.** (a) Cyclic voltammograms of Pt-based metallic glasses compared with pure Pt in 0.01 M $H_2SO_4$ + 0.1 M $Na_2SO_4$ electrolyte at a scan rate of 20 mV/s; (b) cyclic voltammograms of Pd-based metallic glasses compared with pure Pd in 0.01 M $H_2SO_4$ + 0.1 M $Na_2SO_4$ electrolyte at a scan rate of 20 mV/s; (c) UME tip current variation measured by SECM line scans on the surface of the metallic glass alloys compared with pure Pt and Pd.; (d) The average of the UME tip current variation measured by SECM.

current measured from SECM for all the systems studied is plotted in Fig. 3d. Pure Pt and Pd showed the lowest catalytic reactivity towards HOR among all the samples. On the other hand, $Pd_{43}Pt_0$ and $Pt_{57}Pd_0$ amorphous alloys showed higher hydrogen oxidation rates although their noble metal content was significantly lower. The average UME tip current for $Pd_{43}Pt_0$ and $Pt_{57}Pd_0$ amorphous alloys was higher by ~80 nA compared to pure Pt and Pd (Table 1). The metallic glasses containing both Pd and Pt demonstrated the highest activity towards HOR. The average UME tip current for $Pd_{28}Pt_{21}$ and $Pd_{36}Pt_9$ amorphous alloys was higher by ~210 nA compared to pure Pt and Pd (Table 1). Synergistic effects have been demonstrated for noble bimetallic crystalline alloys including Pd–Au catalysts for ethanol oxidation [35] and Pd–Pt catalysts for oxygen reduction [36]. This was attributed to the modification of Pt d-band center and reduced interaction between the Pt atoms and oxygenated species [36]. To explain the synergistic effect seen for the metallic glasses, results from DFT calculations will be discussed in the next section.

The electrochemically active surface area (ECSA) for each alloy was calculated according to the following equation:

$$ECSA\left(m^2 g^{-1}\right) = Q_{H_2} \Big/ \left(Q_{ref} \times [noble\ \ metal]\right) \quad (1)$$

where, $Q_{H_2}$ $(C/m^2)$ is the charge exchanged during hydrogen desorption on the catalyst surface, [noble metal] is the weight percentage of Pt and Pd, and $Q_{ref}$ is the charge required to oxidize a monolayer of hydrogen on the catalyst surface equivalent to 210 μC $cm^{-2}$ on Pt. The reported H adsorption/desorption charge density is calculated based on polycrystalline Pt and averaged over the three

**Table 1**
Electrochemical characterization of the metallic glasses in comparison with pure Pt and Pd.

| Catalyst | Noble metal wt.% | ECSA ($m^2$ $g^{-1}_{metal}$) from CV | Avg. UME tip current from SECM (μA) |
|---|---|---|---|
| Pt | 100 | 4.20 | 0.76 ± 0.02 |
| Pd | 100 | 3.64 | 0.74 ± 0.02 |
| $Pt_{57}Pd_0$ | Pt: 85 | 12.06 | 0.83 ± 0.03 |
| $Pd_{28}Pt_{21}$ | Pd:30, Pt: 43 | 21.43 | 0.97 ± 0.01 |
| $Pd_{36}Pt_9$ | Pd:46, Pt:21 | 19.30 | 0.94 ± 0.01 |
| $Pd_{43}Pt_0$ | Pd: 61 | 11.65 | 0.82 ± 0.04 |

crystalline orientations of (111), (110), and (100) [34,37]. For metallic glasses, there are no crystalline orientations, but the charge density value of 210 μC $cm^{-2}$ was used as the best approximation for the Pt-based amorphous alloy. In the case of Pd-based alloy, the Coulombic charge consumed during $PdO_x$ reduction in the cathodic sweep was used for calculating the ECSA [38,39]. The value of the charge consumed for a monolayer oxide reduction was considered to be 424 μC $cm^{-2}$ [40]. For the catalysts containing both Pt and Pd, the contribution to ECSA for each active element was calculated and added since both elements contribute to the overall electro-catalytic performance. The results of the ECSA calculation are summarized in Table 1. The ECSA value on an average for $Pd_{43}Pt_0$ and $Pt_{57}Pd_0$ amorphous alloys was higher by a factor of three compared to pure Pt and Pd. For the alloys containing both Pt and Pd, $Pd_{28}Pt_{21}$ and $Pd_{36}Pt_9$ metallic glasses, the ECSA value was on an average higher by a factor of five compared to pure Pt and Pd.

### 3.3. Theoretical calculations

To explain the hydrogen oxidation mechanism for the metallic glasses, molecular models were created, as shown in Fig. 4, with compositions identical to the experimentally studied alloys. Since the surface atomic configurations may vary in different regions of the alloy, five different structures were generated for each alloy composition to explore the effect of atomic arrangement on catalytic performance. The overall HOR pathway in acidic solution may be expressed as [41]:

$$H_2 \rightarrow H^* + H^+ + e^- \quad \text{(Reverse Heyrovsky step)} \tag{2}$$

or

$$H_2 \rightarrow H^* + H^* \quad \text{(Reverse Tafel step)} \tag{3}$$

followed by

$$H^* \rightarrow H^+ + e^- \quad \text{(Reverse Volmer step)} \tag{4}$$

where, * refers to the potential active site on the surface and H* denotes the hydrogen atom adsorbed on the surface. The overall oxidation reaction consists of two elementary steps: $H_2$ is decomposed into a proton and H adsorbed on the catalyst surface (H*) by losing an electron, and the desorption of H* to form the second proton after losing another electron [42]. Therefore, catalytic activity for HOR may be determined by calculating the desorption energy of hydrogen from the amorphous alloy surface (Volmer step).

Hydrogen desorption may be considered as the reverse process of hydrogen adsorption. The hydrogen adsorption energy on various compositions of the amorphous alloys was calculated by:

$$\Delta E_{ads} = E_{BMG+H*} - E_{BMG} - \frac{1}{2}E_{H_2} \tag{5}$$

where, $E_{BMG+H*}$is the total energy of metallic glass with H* adsorption, $E_{BMG}$ is the energy of a clean metallic glass surface, and $E_{H_2}$is the energy of hydrogen gas molecules. For “n” hydrogen atoms adsorbed on the surface of the metallic glasses:

$$\Delta E_{n-ads} = \left[E_{BMG+nH*} - E_{BMG} - n*\left(\frac{1}{2}E_{H_2}\right)\right] \Big/ n \tag{6}$$

The Gibbs free energy of hydrogen adsorption may be calculated by the following equation:

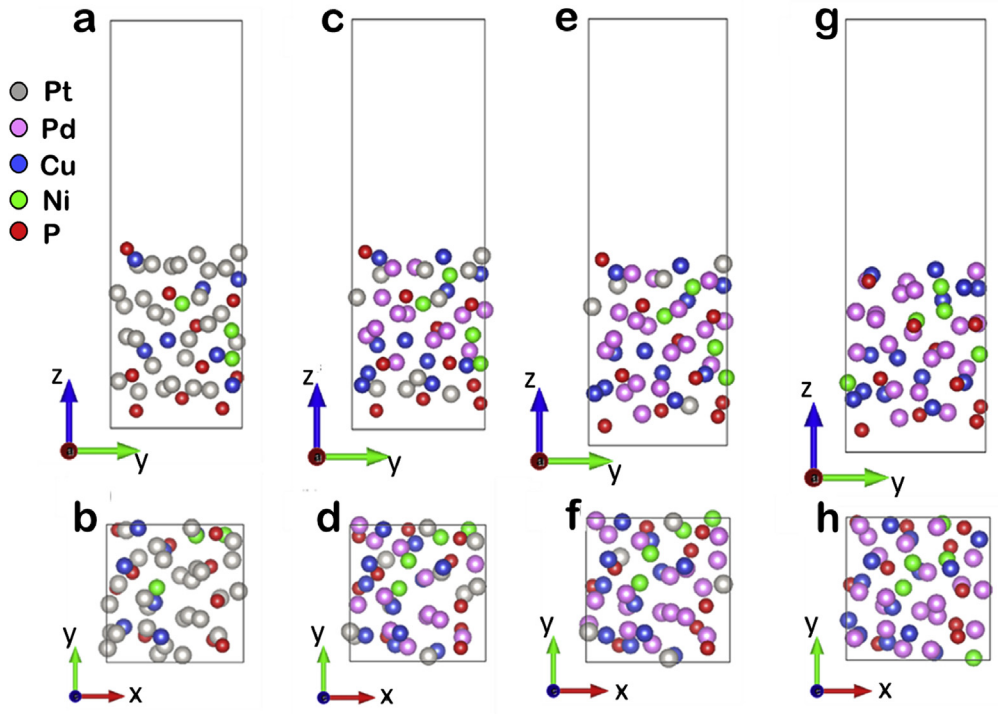


**Fig. 4.** Schematic illustrations of (a) side view and (b) top view of $Pt_{57.5}Cu_{14.7}Ni_{5.3}P_{22.5}$ ($Pt_{57}Pd_0$) metallic glass, (c) side view and (d) top view of $Pd_{27.5}Pt_{20.9}Cu_{22.6}Ni_{8.2}P_{20.9}$ ($Pd_{28}Pt_{21}$), (e) side view and (f) top view $Pd_{36.1}Pt_{9.2}Cu_{25.1}Ni_{9.2}P_{20.3}$ ($Pd_{36}Pt_9$), and (g) side view and (h) top view of $Pd_{43}Ni_{10}Cu_{27}P_{20}$ ($Pd_{43}Pt_0$) metallic glasses. Periodic boundary conditions were applied for all the structures. The silver, blue, green, red and pink circles represent Pt, Cu, Ni, P and Pd, respectively. (For interpretation of the references to colour in this figure legend, the reader is referred to the Web version of this article.)

$$\Delta G_{H^*} = \Delta E_{n-ads} + \Delta E_{ZPE} - T\Delta S \quad (7)$$

where, the $\Delta E_{ZPE}$ is the zero-point energy and $\Delta S$ is the entropy change for hydrogen adsorption. Using the known values for $\Delta E_{ZPE}$ and $\Delta S$, the overall corrections at room temperature may be written as [41]:

$$\Delta G_{H^*} = \Delta E_{n-ads} + 0.24\ eV \quad (8)$$

The over-potential for HOR was calculated by:

$$\eta^{HOR} = \frac{G^{HOR}}{e} \quad (9)$$

where, $G^{HOR} = \max\{\Delta G_1\ ,\ \Delta G_2\}$

Thus, smaller over-potential would indicate higher catalytic activity [41]. An ideal catalyst enables oxidation reaction just above the equilibrium potential with zero over-potential, which may however be difficult due to the binding energies. Lower over-potential would correspond to better performance from a thermodynamic viewpoint and over-potential may be considered as an index representing the energy barrier to overcome in HOR.

Using the first-principles method, the elementary steps of HOR were simulated by introducing H atoms on the amorphous alloy surface. Our calculations show that HOR preferentially follows the reverse Heyrovsky-Volmer pathway instead of the reverse Tafel-Volmer pathway (Fig. 5a). Therefore, the reverse Heyrovsky-Volmer step for the amorphous alloys was the rate-limiting step in HOR. Fig. 5b shows the free energy diagram for the overall HOR process (Reverse Heyrovsky-Volmer pathway) for the four metallic glasses that were experimentally studied. The reaction free energies of pure Pt and Pd [41] are also plotted in Fig. 5b. The figure indicates that the reaction over the surface of $Pd_{28}Pt_{21}$, $Pd_{36}Pd_9$, and $Pt_{57}Pd_0$ metallic glasses was essentially thermo-neutral while this was not the case for $Pd_{43}Pt_0$ alloy and elemental Pt and Pd catalysts. The over-potential for the metallic glasses was relatively lower compared to pure Pt and Pd. Therefore, the enhanced catalytic activity for the metallic glasses towards HOR may be attributed to the reduced chemisorption of hydrogen on the catalyst surface.

Adsorption energy was calculated for different degrees of hydrogen coverage on the surface of the metallic glasses. Fig. 6a shows the adsorption energy of hydrogen with coverage of 25% and 100% for each of the amorphous alloys. The adsorption energy was found to increase with increasing coverage, consistent with the trend reported for pure Pt [41]. Hydrogen oxidation reaction (HOR) typically proceeds under high proton coverage. Therefore, 100% of hydrogen coverage was used for the calculation of the minimum value of over-potential for different structures of the same alloy to represent the catalytic performance. The minimum value of over-potential for each metallic glass is shown in Fig. 6b and compared with pure Pt and Pd. The results show that $Pd_{27.5}Pt_{20.9}Cu_{22.6}Ni_{8.2}P_{20.9}$ ($Pd_{28}Pt_{21}$) and $Pd_{36.1}Pt_{9.2}Cu_{25.1}Ni_{9.2}P_{20.3}$ ($Pd_{36}Pt_9$) have very low over-potential, almost close to zero. Compared with pure Pt and Pd, over-potentials for the amorphous alloys were found to be significantly lower. This trend obtained from the DFT calculations is consistent with the experimental results shown in Fig. 3. The high catalytic activity of the amorphous alloys likely originates from the synergistic effect between Pt and Pd due to electronic band structure modification and lowering of work function (WF) [43]. Work function is defined as the minimum energy required to remove an electron from the surface of a material and shown to be directly correlated with charge transfer and catalytic activity [44,45]. Work function has been correlated with the activity of heterogeneous catalysts in several important catalytic reactions including oxygen reduction reaction (ORR) [46], ammonia synthesis [47], $N_2O$ decomposition [48], and hydrogen evolution reaction (HER) [49]. Scanning Kelvin Probe (SKP) measurements for the metallic glasses used in this study showed that WF was lower for the amorphous alloys compared with pure Pt and Pd [43]. In addition to lower WF, binding energy of Pt and Pd core levels was relatively higher for the metallic glasses compared with pure Pt and Pd [43], which determines the activation energy for hydrogen oxidation [50]. The DFT calculations strongly support the experimental findings that the amorphous alloys containing both Pd and Pt exhibited the highest activity towards HOR among all the metallic glasses studied, although they contained significantly lower amounts of noble metal.

## 4. Conclusions

The electro-catalytic performance of recently developed noble metal-based bulk metallic glasses towards hydrogen oxidation reaction was studied using cyclic voltammetry and scanning electrochemical microscopy. All the metallic glasses showed much higher catalytic current density compared with pure crystalline Pt and Pd under identical experimental conditions. The amorphous alloys containing both Pt and Pd showed the best performance. Gibbs's free energy for hydrogen adsorption was calculated using DFT for molecular models of composition identical to the experiments. The DFT calculations were in good agreement with

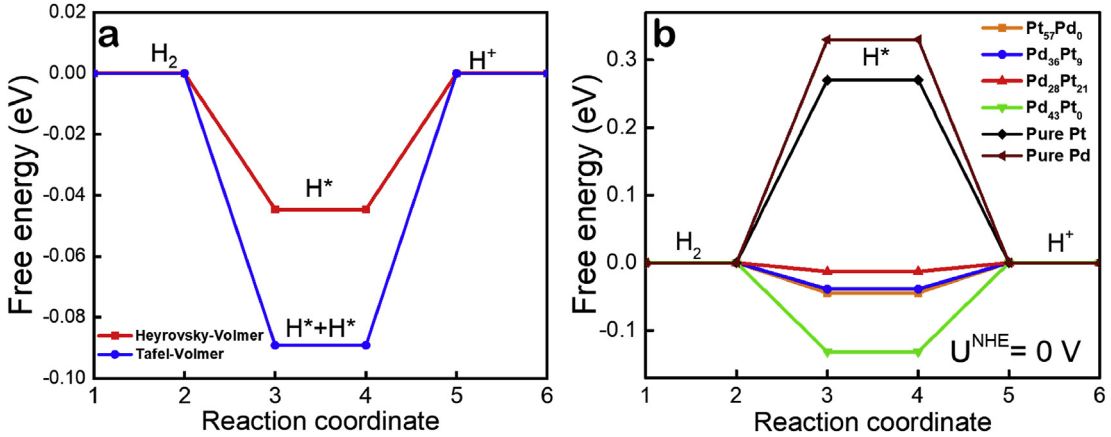


**Fig. 5.** (a) Free energy diagram for overall hydrogen oxidation at equilibrium for $Pt_{57}Pd_0$ metallic glass through different pathways; (b) Free energy diagram with Reverse Heyrovsky-Volmer pathway for the typical metallic glass structures (100% adsorbate (H) coverage) and at a potential U = 0 V relative to the normal hydrogen electrode (NHE).

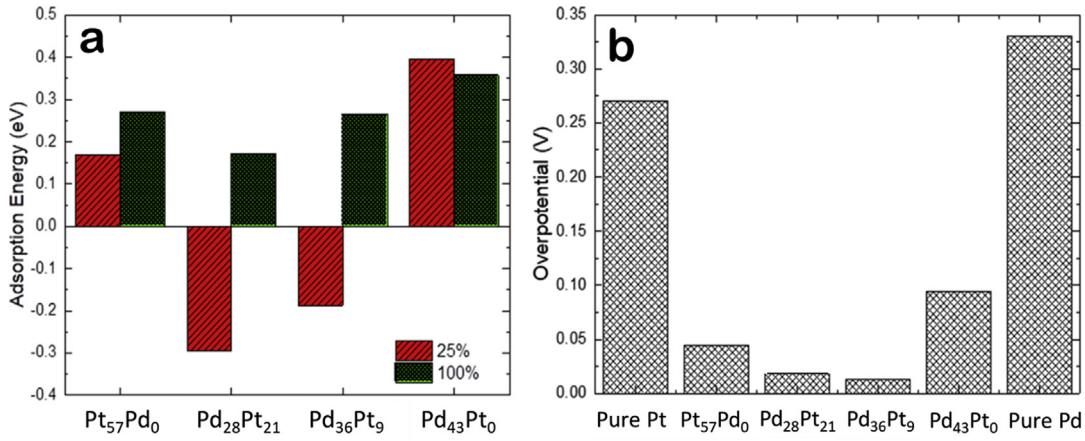


**Fig. 6.** (a) Gibbs free energy for hydrogen adsorption for four metallic glass structures, $Pt_{57}Pd_0$, $Pd_{28}Pt_{21}$, $Pd_{36}Pt_9$, and $Pd_{43}Pt_0$, with hydrogen coverage of 25% and 100%; (b) Minimum values of the over-potential for the four metallic glass catalysts with 100% hydrogen coverage (values for pure Pd and Pt are also added based on reference [41]).

experimental findings on the trend of catalytic activity and hydrogen adsorption energy. Weakened chemisorption of hydrogen on the surface of the amorphous alloys promoted higher catalytic activity towards hydrogen oxidation compared to pure Platinum and Palladium.

## Credit author statement

V. Hasannaeimi: Conceptualization, Methodology, Investigation, Writing - original draft, Writing - review & editing. C-Y. Lin: Computations, Investigation, Writing - review & editing. Z. Xia: Conceptualization, Validation, Writing - review & editing. S. Mukherjee: Conceptualization, Supervision, Funding acquisition, Validation, Writing - review & editing.

## Declaration of competing interest

The authors declare that they have no known competing financial interests or personal relationships that could have appeared to influence the work reported in this paper.

## Acknowledgments

This work was partly supported by funding from the National Science Foundation (NSF) under grant numbers 1561886, 1919220, and 1762545. Any opinions, findings, and conclusions expressed in this paper are those of the authors and do not necessarily reflect the views of the National Science Foundation (NSF). The authors also acknowledge the Materials Research Facility (MRF) and Advanced Materials and Manufacturing Processes Institute (AMMPI) at the University of North Texas for the characterization facilities.

## References

[1] M. Momirlan, T.N. Veziroglu, The properties of hydrogen as fuel tomorrow in sustainable energy system for a cleaner planet, Int. J. Hydrogen Energy 30 (7) (2005) 795–802.
[2] E.L. Miller, S.T. Thompson, K. Randolph, Z. Hulvey, N. Rustagi, S. Satyapal, US Department of Energy hydrogen and fuel cell technologies perspectives, MRS Bull. 45 (1) (2020) 57–64.
[3] N. Cheng, et al., Platinum single-atom and cluster catalysis of the hydrogen evolution reaction, Nat. Commun. 7 (2016) 13638.
[4] A. Faur Ghenciu, Review of fuel processing catalysts for hydrogen production in PEM fuel cell systems, Curr. Opin. Solid State Mater. Sci. 6 (5) (2002) 389–399.
[5] R. Subbaraman, et al., Enhancing hydrogen evolution activity in water splitting by tailoring Li+-Ni (OH) 2-Pt interfaces, Science 334 (6060) (2011) 1256–1260, 80.
[6] H. Yin, et al., Ultrathin platinum nanowires grown on single-layered nickel hydroxide with high hydrogen evolution activity, Nat. Commun. 6 (2015) 6430.
[7] J. Zhang, PEM Fuel Cell Electrocatalysts and Catalyst Layers: Fundamentals and Applications, Springer Science & Business Media, 2008.
[8] M.M.P. Janssen, J. Moolhuysen, "Binary systems of platinum and a second metal as oxidation catalysts for methanol fuel cells," *Electrochim*, Acta 21 (11) (1976) 869–878.
[9] M. Götz, H. Wendt, Binary and ternary anode catalyst formulations including the elements W, Sn and Mo for PEMFCs operated on methanol or reformate gas, Electrochim. Acta 43 (24) (1998) 3637–3644.
[10] P. Strasser, et al., "Lattice-strain control of the activity in dealloyed core–shell fuel cell catalysts, Nat. Chem. 2 (6) (2010) 454.
[11] Z. Wen, J. Liu, J. Li, "Core/shell Pt/C nanoparticles embedded in mesoporous carbon as a methanol-tolerant cathode catalyst in direct methanol fuel cells, Adv. Mater. 20 (4) (2008) 743–747.
[12] S. Sun, et al., Single-atom catalysis using Pt/graphene achieved through atomic layer deposition, Sci. Rep. 3 (2013) 1775.
[13] M. Simões, S. Baranton, C. Coutanceau, Electro-oxidation of glycerol at Pd based nano-catalysts for an application in alkaline fuel cells for chemicals and energy cogeneration, Appl. Catal. B Environ. 93 (3–4) (2010) 354–362.
[14] S. Sun, F. Jaouen, J. Dodelet, Controlled growth of Pt nanowires on carbon nanospheres and their enhanced performance as electrocatalysts in PEM fuel cells, Adv. Mater. 20 (20) (2008) 3900–3904.
[15] S. Mukherjee, R.C. Sekol, M. Carmo, E.I. Altman, A.D. Taylor, J. Schroers, Tunable hierarchical metallic-glass nanostructures, Adv. Funct. Mater. 23 (21) (Jun. 2013) 2708–2713.
[16] J. Li, G. Doubek, L. McMillon-Brown, A.D. Taylor, Metallic glass nanostructures: recent advances in metallic glass nanostructures: synthesis strategies and electrocatalytic applications (adv. Mater. 7/2019, Adv. Mater. 31 (7) (Feb. 2019) 1970050.
[17] S. Mukherjee, M. Carmo, G. Kumar, R.C. Sekol, A.D. Taylor, J. Schroers, Palladium nanostructures from multi-component metallic glass, Electrochim. Acta 74 (2012) 145–150.
[18] J. Schroers, Processing of bulk metallic glass, Adv. Mater. 22 (14) (2010) 1566–1597.
[19] R.C. Sekol, et al., Pd-Ni-Cu-P metallic glass nanowires for methanol and ethanol oxidation in alkaline media, Int. J. Hydrogen Energy 38 (26) (2013) 11248–11255.
[20] M. Carmo, R.C. Sekol, S. Ding, G. Kumar, J. Schroers, A.D. Taylor, Bulk metallic glass nanowire architecture for electrochemical applications, ACS Nano 5 (4) (2011) 2979–2983.
[21] M. Zhao, K. Abe, S. Yamaura, Y. Yamamoto, N. Asao, "Fabrication of Pd–Ni–P metallic glass nanoparticles and their application as highly durable catalysts in methanol electro-oxidation, Chem. Mater. 26 (2) (Jan. 2014) 1056–1061.
[22] A. Baiker, Metallic glasses in heterogeneous catalysis, Faraday Discuss. Chem. Soc. 87 (1989) 239–251.
[23] J. Schroers, W.L. Johnson, Highly processable bulk metallic glass-forming alloys in the Pt–Co–Ni–Cu–P system, Appl. Phys. Lett. 84 (18) (Apr. 2004) 3666–3668.
[24] N. Nishiyama, A. Inoue, Supercooling investigation and critical cooling rate for glass formation in Pd–Cu–Ni–P alloy, Acta Mater. 47 (5) (1999) 1487–1495.
[25] G. kresse, d. joubert, From ultrasoft pseudopotentials to the projector augmented-wave method, Phys. Rev. B 59 (1999) 1758.
[26] P.E. Blöchl, Projector augmented-wave method, Phys. Rev. B 50 (24) (1994) 17953.
[27] G. Kresse, J. Furthmüller, Efficient iterative schemes for ab initio total-energy calculations using a plane-wave basis set, Phys. Rev. B 54 (1996) 11169.

[28] G. Kresse, J. Furthmiller, Efficiency of ab-initio total energy calculations for metals and semiconductors using a plane-wave basis set, Comput. Mater. Sci. 6 (1) (1996) 15–50.
[29] P. Zoltowski, E. Makowska, Diffusion coefficient of hydrogen in α-phase palladium and palladium-platinum alloy, Phys. Chem. Chem. Phys. 3 (14) (2001) 2935–2942.
[30] M.S. Rau, P.M. Quaino, M.R.G. de Chialvo, A.C. Chialvo, "Hydrogen oxidation reaction: evidences of different electrocatalytic activity between α and β Pd–H, Electrochem. Commun. 10 (2) (2008) 208–212.
[31] C. Gabrielli, P.P. Grand, A. Lasia, H. Perrot, Investigation of hydrogen adsorption and absorption in palladium thin films II. Cyclic voltammetry, J. Electrochem. Soc. 151 (11) (2004) A1937–A1942.
[32] F. Alcaide, G. Álvarez, P.L. Cabot, O. Miguel, A. Querejeta, Performance of carbon-supported PtPd as catalyst for hydrogen oxidation in the anodes of proton exchange membrane fuel cells, Int. J. Hydrogen Energy 35 (20) (2010) 11634–11641.
[33] C. Wei, A.J. Bard, M. V Mirkin, Scanning electrochemical microscopy. 31. Application of SECM to the study of charge transfer processes at the liquid/liquid interface, J. Phys. Chem. 99 (43) (1995) 16033–16042.
[34] W. Li, A.M. Lane, Resolving the HUPD and HOPD by DEMS to determine the ECSA of Pt electrodes in PEM fuel cells, Electrochem. Commun. 13 (9) (2011) 913–916.
[35] F. Cheng, X. Dai, H. Wang, S.P. Jiang, M. Zhang, C. Xu, Synergistic effect of Pd–Au bimetallic surfaces in Au-covered Pd nanowires studied for ethanol oxidation, Electrochim. Acta 55 (7) (2010) 2295–2298.
[36] B. Lim, et al., Pd-Pt bimetallic nanodendrites with high activity for oxygen reduction, Science 324 (5932) (2009) 1302–1305.
[37] T. Biegler, D.A.J. Rand, R. Woods, Limiting oxygen coverage on platinized platinum; Relevance to determination of real platinum area by hydrogen adsorption, J. Electroanal. Chem. 29 (2) (1971) 269–277.
[38] T. Maiyalagan, A.B.A. Nassr, T.O. Alaje, M. Bron, K. Scott, Three-dimensional cubic ordered mesoporous carbon (CMK-8) as highly efficient stable Pd electro-catalyst support for formic acid oxidation, J. Power Sources 211 (2012) 147–153.
[39] H. Duncan, A. Lasia, Mechanism of hydrogen adsorption/absorption at thin Pd layers on Au(111), Electrochim. Acta 52 (21) (2007) 6195–6205.
[40] T.R. Soreta, J. Strutwolf, O. Henry, C.K. O'Sullivan, Electrochemical surface structuring with palladium nanoparticles for signal enhancement, Langmuir 26 (14) (2010) 12293–12299.
[41] J.K. Nørskov, et al., Trends in the exchange current for hydrogen evolution, J. Electrochem. Soc. 152 (3) (2005) J23–J26.
[42] Y. Zheng, et al., Hydrogen evolution by a metal-free electrocatalyst, Nat. Commun. 5 (2014) 3783.
[43] V. Hasannaeimi, S. Mukherjee, noble-Metal based Metallic Glasses as Highly catalytic Materials for Hydrogen oxidation Reaction in fuel cells, Sci. Rep. 9 (1) (2019) 1–8.
[44] A. Maljusch, J.B. Henry, J. Tymoczko, A.S. Bandarenka, W. Schuhmann, Characterisation of non-uniform functional surfaces: towards linking basic surface properties with electrocatalytic activity, RSC Adv. 4 (4) (2014) 1532–1537.
[45] K. Yokoyama, et al., Work function, carrier type, and conductivity of nitrogen-doped single-walled carbon nanotube catalysts prepared by annealing via defluorination and efficient oxygen reduction reaction, Carbon N. Y. 142 (2019) 518–527.
[46] J. Duch, P. Stelmachowski, A.H.A.M. Videla, M. Gajewska, A. Kotarba, S. Specchia, Thermal oxygen activation followed by in situ work function measurements over carbon-supported noble metal-based catalysts, Int. J. Hydrogen Energy 44 (31) (2019) 16648–16656.
[47] M. Reli, et al., Novel cerium doped titania catalysts for photocatalytic decomposition of ammonia, Appl. Catal. B Environ. 178 (2015) 108–116.
[48] G. Grzybek, et al., Insights into the twofold role of Cs doping on deN2O activity of cobalt spinel catalyst—towards rational optimization of the precursor and loading, Appl. Catal. B Environ. 168–169 (2015) 509–514, https://doi.org/10.1016/j.apcatb.2015.01.005.
[49] Z.W. Seh, J. Kibsgaard, C.F. Dickens, I.B. Chorkendorff, J.K. Nørskov, T.F. Jaramillo, Combining theory and experiment in electrocatalysis: insights into materials design, Science 355 (6321) (2017) eaad4998.
[50] Q. Zhao, et al., Synthesis of highly active and dual-functional electrocatalysts for methanol oxidation and oxygen reduction reactions, Appl. Surf. Sci. 389 (2016) 181–189.